Deficient synaptic neurotransmission results in a persistent sleep-like cortical activity across vigilance states in mice

Mathilde C. C. Guillaumin[1,2,3], Christian D. Harding[2,4], Lukas B. Krone[2,4,5], Tomoko Yamagata[1,2], Martin C. Kahn[2,4], Cristina Blanco-Duque[2,4], Gareth T. Banks[6], Patrick M. Nolan[6], Stuart N. Peirson[1,2], Vladyslav V. Vyazovskiy[2,4].

[1] Nuffield Department of Clinical Neurosciences, University of Oxford, Oxford, UK.

[2] Kavli Institute for Nanoscience Discovery, Sleep and Circadian Neuroscience Institute, University of Oxford, Oxford, UK.

[3] Medical Research Council Brain Network Dynamics Unit, Nuffield Department of Clinical Neurosciences, University of Oxford, Oxford, UK.

[4] Department of Physiology, Anatomy and Genetics, University of Oxford, Oxford, UK.

[5] University Hospital of Psychiatry and Psychotherapy, University of Bern, Switzerland

[6] Mammalian Genetics Unit, MRC Harwell Institute, Harwell Science and Innovation Campus, Oxfordshire, UK.

Corresponding author(s): vladyslav.vyazovskiy@dpag.ox.ac.uk.

ABSTRACT

Growing evidence suggests that brain activity during sleep, as well as sleep regulation, are tightly linked with synaptic function and network excitability at the local and global levels. We previously reported that a mutation in synaptobrevin 2 (*Vamp2*) in restless (*rlss*) mice results in a marked increase of wakefulness and suppression of sleep, in particular REM sleep (REMS) as well as increased consolidation of sleep and wakefulness. In the current study, using finer-scale *in vivo* electrophysiology recordings, we report that spontaneous cortical activity in *rlss* mice during NREM sleep (NREMS) is characterised by an occurrence of abnormally prolonged periods of complete neuronal silence (OFF-periods), often lasting several seconds, similar to the burst suppression pattern typically seen under deep anaesthesia. Increased incidence of prolonged network OFF-periods was not specific to NREMS, but also present in REMS and wake in *rlss* mice. Slow-wave activity (SWA) was generally increased in *rlss* mice, while higher frequencies including theta-frequency activity were decreased, further resulting in diminished differences between vigilance states. The relative increase in SWA after sleep deprivation was attenuated in *rlss* mice, suggesting either that *rlss* mice experience persistently elevated sleep pressure, or, alternatively, that the intrusion of sleep-like patterns of activity into awake state diminishes the accumulation of sleep drive. We propose that deficit in global synaptic neurotransmitter release leads to 'state inertia', reflected in an abnormal propensity of brain networks to enter and remain in a persistent 'default state' resembling coma or deep anaesthesia.

KEYWORDS

Sleep, sleep homeostasis, sleep-wake control/regulation, synaptobrevin 2, VAMP2, sleep architecture, neural inertia, state inertia.

INTRODUCTION

Despite recent advances in our understanding of neurophysiological and molecular mechanisms of sleep-wake control, it remains unclear how sleep and wake alternation is regulated at a brain-wide scale, and whether such fundamental aspects of neuronal function as synaptic release have a role to play in that respect.

The restless (*rlss*) mouse line, obtained via a forward genetics sleep screen and possessing a mutation in synaptobrevin 2/*Vamp2* (a gene encoding the key synaptic-release machinery protein VAMP2) showed an array of sleep and behavioural phenotypes (Banks et al., 2020), including a decreased amount of NREM sleep (NREMS) in the dark phase, alongside an overall decrease in REM sleep (REMS) time. More strikingly, the number of sleep and wake episodes and of state transitions was markedly reduced in *rlss* mice, correlating with increased duration of episodes in all vigilance states compared to littermate controls. The probability to transition from one state to the next in normal conditions was found to be markedly reduced in *rlss* mice, leading to a general 'vigilance state inertia'.

The mutation in *Vamp2* results in a markedly decreased neurotransmitter release probability in *rlss* mice, altering synaptic transmission (Banks et al., 2020). These findings raised two questions. First, why did this state-transitioning probability decrease for all states, and in both directions between two given states (except NREMS-to-wake transitions)? Secondly, what are the underpinning mechanisms of the decrease in time spent in REMS? Having shown changes in the architecture of vigilance states (Banks et al., 2020), we now take a different approach and look at the 'quality' of the states themselves, to address the question of whether changes in state dynamics and architecture between *rlss* and wild-type (WT) mice induce qualitative differences between states.

EEG slow-wave activity (SWA), which corresponds to the EEG power in the slow-wave frequency range (0.5-4 Hz) in NREMS, has been a useful measure to evaluate sleep-wake dynamics. Slow-waves tend to dominate the EEG during NREMS and can be recorded across the entire cortical surface (Massimini et al., 2004; Steriade et al., 1993). Both animal and human studies have shown that SWA levels are closely linked to sleep-wake history, where SWA levels at the onset of NREMS positively correlate with preceding time spent awake, and levels subsequently decrease during NREMS (Achermann and Borbely, 2003; Borbely et al., 1984). SWA has therefore been traditionally used as a marker of sleep pressure (Borbely et al., 1981; Dijk et al., 1987). However, EEG records global signals across the cortical surface. Local field potentials (LFP) and multi-unit activity (MUA) instead allow us to look at sleep-wake dynamics at a more local level. In addition, as the initiation of slow-waves (depth positive/surface negative deflections) correspond to periods of neuronal silence (Calvet et al., 1973; Contreras and Steriade, 1995; Harding et al., 2023; Mukovski et al., 2007; Steriade et al., 1993; Steriade et al., 2001; Vyazovskiy et al., 2009), which also depend on the levels of network synchrony (Vyazovskiy et al., 2009), multi-unit activity allows us to investigate the underlying patterns of neuronal silence ('OFF-periods') (Harding et al., 2023).

In the present study, we used EEG, LFP and MUA recordings, combined with sleep deprivation and auditory stimulation paradigms, to gain a better understanding of the sleep depth of *rlss* mice. Auditory stimuli are commonly used to investigate sleep depth, sensory dissociation during sleep and arousal thresholds from NREMS and REMS (Hayat et al., 2022; Neckelmann and Ursin, 1993; Nir et al.,

2015; Rechtschaffen et al., 1966; Wimmer et al., 2012). We investigated the spectral signature of global sleep and wake states, in particular at state transitions. We further explored the neuronal dynamics underlying the marked behavioural changes observed, and, using a mathematical model of sleep regulation (Guillaumin et al., 2018; Thomas et al., 2020), we examined the homeostatic regulation of sleep in *rlss* mice. We found that in *rlss* mice, the boundaries between electrophysiological signatures of vigilance states were less distinct than in control animals, and that sleep homeostasis dynamics were altered, with *rlss* mice being slower to dissipate accumulated sleep pressure. This was not associated, however, with an altered responsiveness to external sensory stimuli such as a sound.

This study suggests that impaired neurotransmitter release leads to an increased propensity to revolve around a 'default state' of cortical activity (Bandarabadi et al., 2020; Buzsáki, 2006; Lemieux et al., 2014; Sanchez-Vives et al., 2017; Sanchez-Vives and Mattia, 2014; Timofeev et al., 2020), with important consequences for global and local sleep architecture and sleep homeostasis.

RESULTS

***rlss* mice show increased propensity for hybrid states of vigilance.**

Using EEG combined with LFP recordings in freely-moving mice from the motor (M1) and visual (V1) cortical areas (**Figure 1a**), we found that *rlss* mice have an increase in spectral power in the very low frequencies in NREMS and REMS and a decrease in the higher frequency bins in REMS (EEG only), NREMS and Wake (**Figures 1b and S1a**). Interestingly, the differences between *rlss* and WT mice' spectral signatures diverged between the frontal EEG and LFP signals in REMS, with an increase in the very-low delta band and theta (and higher) frequencies in the frontal REMS EEG, and an increase in the upper delta band in the frontal LFP in *rlss* mice compared to WT mice (**Figure 1b, middle**). Changes in the EEG occipital derivation paralleled the ones observed in the frontal EEG (**Figure S1a**); therefore, as LFP signals were recorded from M1, we also focused on EEG signals from this region (frontal). Local cortical dynamics thus revealed a disparity between local intracortical and brain surface ('global') signatures of REMS in *rlss* mice.

LFP signals in *rlss* mice were also characterised by a decrease in their amplitude, especially during NREMS, when traces were reminiscent of the burst suppression patterns that are typically observed during general anaesthesia, but also coma, hypothermia and some early infantile pathologies (Brown et al., 2010; Clark and Rosner, 1973; Huang et al., 2021; Shanker et al., 2021) (**Figure 1c and Movie 1**). Such EEG/LFP signatures across vigilance states indicate that sleep inertia not only means fewer state transitions in *rlss* mice (Banks et al., 2020), but also that they display an intrusion of default-mode-like traits (Sanchez-Vives et al., 2017) across all states of vigilance, with the well-known spectral signatures of NREMS, REMS and wake being affected. The boundaries between states' typical signatures appear less distinct in *rlss* mice, due to an increased power in the very slow frequencies not only in NREMS, but also in REMS and wake, associated with a decreased theta power in REMS in *rlss* mice. At a finer time resolution, looking at spectrograms at the transitions from NREMS to REMS, we found typical differences between *rlss* and WT mice. Blurred boundaries between states in *rlss* mice appeared all

124 the more evident, with the drop in spectral power in the slow-frequency range (0.5-4 Hz) that is usually
125 observed at NREMS-to-REMS transitions being significantly reduced in *rlss* mice (**Figures 1d,e**).

126

127 ***rlss* mice show prolonged periods of neuronal silence across all vigilance states, and especially**
128 **during NREMS, reminiscent of burst suppression patterns.**

129 These EEG and LFP results raised the following question: what is it in the brain activity of *rlss* mice that
130 is different for such sleep-architecture and spectral variations to arise? Using MUA recordings and our
131 recently developed 'OFF-period' detection algorithm (Harding et al., 2023), we discovered that
132 neuronal firing in *rlss* mice ceases for seconds at a time during NREMS, in a locally synchronised
133 manner (**Figure 2a and Movie 1**). Compared to WTs, in *rlss* animals, periods of such synchronised
134 neuronal silence ('OFF-periods') lasted significantly longer and coincided with very low-amplitude,
135 nearly isoelectric EEG and LFP traces (**Figure 2a,b and Movie 1**). Importantly, this also held true in
136 REMS and wake when OFF-periods were generally longer in *rlss* mice (**Figure 2b**).

137 As a next step, we aimed to specifically investigate the longest OFF-periods, and thus selected the 5%
138 longest OFF-periods which we looked at separately (see Methods). We found that OFF-periods are
139 significantly longer in *rlss* mice, being about twice as long as in WT during NREMS (**Figure 2c**); this
140 further supports a state of 'neuronal inertia', whereby in *rlss* mice neurons are less likely to resume
141 activity upon a period of silence of a certain duration.

142 As we previously hypothesised (Banks et al., 2020), it seems that changes in synaptic vesicular release
143 lead to changes in cellular and network excitability which, by altering excitatory-inhibitory balance
144 between cell populations controlling sleep and wake states, result in changes in sleep architecture.
145 However, firing rates detected from MUA were not significantly altered (**Figure S1b**). This may also
146 underlie the 'default state' features prominent in all vigilance states, leading to an increased
147 uniformity in their spectral characteristics, particularly striking at state transitions (**Figure 1b,d,e**). We
148 argue that transitions between active and silent states at the level of individual cells and networks
149 may lag behind global state transitions, resulting in a longer time spent in mixed, hybrid states of
150 vigilance.

151 Given this 'neuronal' inertia that may underlie the less clear-cut boundaries between vigilance state
152 signatures, and the alterations in EEG and LFP spectra, notably in the slow-wave frequency range –
153 which is traditionally used to investigate sleep homeostasis dynamics – we next asked whether sleep
154 homeostasis was affected in *rlss* mice.

155

156 **Sleep homeostasis is generally conserved in *rlss* mice, with increased sleep quantity but not sleep**
157 **quality, in response to sleep deprivation.**

158 To investigate the sleep homeostatic response in *rlss* mice we subjected the mice to a 6-h sleep
159 deprivation protocol starting at light onset (time/Zeitgeber 0 - ZT0), after which the mice were left
160 undisturbed for the subsequent 18h. Following this 6-h sleep deprivation period, *rlss* mice showed a
161 markedly decreased sleep latency compared to their WT littermates (**Figure 3a**). This is the only case
162 when we observed state switching probability being greater in *rlss* mice compared to WTs. The time
163 spent in NREMS in the 6h following SD was increased by an 1h in *rlss* animals compared to WTs, while
164 REMS time was halved (**Figures 3b-d**). However, across the whole recovery period (18h post sleep-

deprivation), baseline comparative sleep structure was restored, with *rlss* mice spending less time in both NREMS and REMS than WT mice (**Figure 3d, right**). At the end of this 18-h recovery period, all mice had reached their baseline daily levels of NREMS and REMS (**Figures 3b,c**).

SWA, the power in the delta (0.5-4Hz)-frequency range is a common marker of sleep need and sleep 'efficiency'. Here, we found that the relative increase in SWA commonly triggered by sleep deprivation was markedly reduced in *rlss* mice (**Figures 3e and S2**). This was the case for both the EEG and LFP signals, and was particularly marked in the 2h directly following sleep deprivation (**Figures 3e,f and S2**). This indicates that although sleep homeostasis is partly conserved in *rlss* mice (the time taken to reach baseline levels of NREMS and REMS is comparable between genotypes – **Figure 3b,c**), SWA, reflecting sleep pressure, does not build up at the same rate in *rlss* mice. To summarise, *rlss* mice are able to compensate for sleep loss in a similar amount of time to WT mice (**Figures 3b,c**), but this is made possible by spending more time asleep (**Figure 3d**), as their increase in SWA during recovery NREMS (which allows for sleep pressure dissipation) is lower compared to their own baseline levels (**Figures 3e,f and S2**). In short, there seems to be a trade-off between sleep quantity (duration spent sleeping) and sleep quality (higher SWA levels) in those mice following a sleep deprivation challenge.

The fact that their baseline SWA levels is higher (possibly due to neuronal inertia) may also explain, firstly, why they sleep less overall during a baseline day, and secondly, why the relative increase in SWA following sleep deprivation is dampened. Indeed, there could be a ceiling effect with longer, more synchronised periods of neuronal silence not being possible as they are already long under baseline conditions. Therefore, a further increase in SWA (which reflects larger-amplitude, slow-frequency deflections in the signal and is thus a read-out of synchronized periods of neuronal silence and firing) may be limited. We observed that OFF-period durations following sleep deprivation did not increase in *rlss* mice, but nor did they in WT mice (**Figure 3h-i**). This can be expected as changes in the average duration of OFF-periods naturally occur between baseline and sleep deprivation conditions in WT animals (Vyazovskiy et al., 2009); therefore genotype-specific changes may be more easily observable in terms of incidence (**Figure 3g**) than duration. This may also be explained by the fact that here, we chose to analyse the longest OFF-periods and combine early and late sleep. Yet, early sleep usually contains longer OFF-periods than later sleep (McKillop et al., 2018; Vyazovskiy et al., 2009). No significant changes in OFF-period duration in REMS was observed in either WT or *rlss* mice in response to sleep deprivation (**Figure 3j-l**).

The fact that the increase in SWA is dampened in *rlss* mice compared to WT mice following sleep deprivation may either arise from *rlss* mice experiencing chronically elevated sleep pressure, thus leaving less capacity for a further increase in response to sleep deprivation. Or, it may be that as the neural activity of *rlss* mice persistently revolves around a default state, they do not accumulate sleep pressure as steeply as WT mice during waking (Thomas et al., 2020). To investigate this further, we used an adapted version of the 'two-process model' of sleep regulation that we have previously described (Guillaumin et al., 2018).

Response to sleep deprivation in *rlss* mice reveals a decreased sleep quality that is compensated for by an increase in sleep quantity.

To investigate the dynamics of SWA and sleep homeostasis in *rlss* mice, we applied the two-process model of sleep regulation (Achermann et al., 1993; Guillaumin et al., 2018) to recordings obtained in *rlss* and WT mice. This model predicts the levels of SWA across a 24-h day, given the hypnogram (vigilance states) of a mouse. We optimised the parameters of the model for each mouse against a baseline day (see Methods). The model's predictions were satisfactory (squared error <10% at the end of the optimisation, see methods in Guillaumin et al. (2018)) but variable across mice (**Figure 4a**). In particular, the fit was poorer overall in WT mice (higher variations in the squared errors obtained at the end of the optimisation stage). This could stem from a more fragmented sleep-wake architecture in those animals, as opposed to *rlss* mice, which have more consolidated bouts of sleep and wakefulness due to their state inertia phenotype. As the model tends to perform better when faced with longer wake bouts (which present a 'challenge' to the model as they lead to higher subsequent SWA), we next performed another set of optimisations using 24 h of baseline followed by a sleep deprivation day (6 h sleep deprivation and 18 h recovery).

When comparing the results obtained with both approaches (BL only vs. BL+SD day), we found that the parameter values obtained with either approach were overall similar, except when optimisations were run against LFP data (**Figure 4b**). This suggests that the equations are better designed to fit EEG, from which they were initially derived (Guillaumin et al., 2018), than LFP signals. *rlss* mice had significantly reduced values of gc (gain constant, the rate of decrease of SWA) and S_U (upper asymptote of SWA levels) in both EEG derivations (**Figure 4b, upper and middle panels**), but not LFP (**Figure 4b, lower panels**). The results therefore suggest that the rate at which sleep pressure decreases in *rlss* mice (gc) is slower, but that the upper threshold to which sleep pressure can build-up (S_U) is also lower. These findings should nevertheless be interpreted bearing in mind the model relies on power in the slow-wave range during NREMS (SWA), which is affected by the very low-amplitude oscillations observed in *rlss*, as described above.

Putting these results in perspective with our earlier findings, knowing that *rlss* mice have a reduced total sleep time, one could hypothesize a more efficient sleep, which would be reflected in a higher decay rate (higher gc), or hypothesize a slower build-up (lower rs) of sleep pressure during wake. Yet, we observed the opposite findings, with a significantly decreased decay rate in *rlss* mice compared to WTs, and no significant difference in the rise constant rs (**Figure 4b**). These results held true in both EEG derivations, but not in the LFP recordings. On the other hand, *rlss* mice were characterized by a significantly reduced upper asymptote S_U. This could explain how *rlss* mice come back to baseline levels of sleep (**Figure 3b,c**) in the same amount of time as WT mice despite a slower dissipation of sleep pressure, given that they start with lower levels (as shown by a lower upper asymptote).

Taken together, computational modelling provided additional insight into the sleep homeostasis dynamics in *rlss* mice. Our data suggest that efficient sleep pressure dissipation requires intact neuronal dynamics, i.e. rate of shifting between quiescent and firing states, which is impaired in *rlss* mice. On the other hand, consolidated bouts of sleep, which *rlss* mice display, would not lead to better sleep pressure dissipation according to our model. In addition, these results support the idea that as *rlss* mice have intrusions of default-state/sleep-like patterns during wake (and REMS), they do not build sleep pressure as readily (Thomas et al., 2020). This is supported by our finding of a significantly reduced upper asymptote level, leading to a decreased need for sleep pressure dissipation.

Conserved behavioural reaction to auditory stimuli, but altered response at the neuronal level, in *rlss* mice.

Finally, given the inertia shown by *rlss* mice to switch between states, both at the behavioural and neuronal levels, we asked whether their response to external stimuli – such as a sound – could be impaired too. We wanted to address whether the elevated power in the slow-wave range and the ceiling effect (smaller increase) in SWA following sleep deprivation could reflect a higher sleep depth in *rlss* mice, which would lead to a higher arousal threshold. Using an auditory stimulation paradigm (**Figure 5a**), we found that the number of full arousals (i.e. the mouse stays awake for at least 16 sec after the sound, see Methods) following the sounds was similar across genotypes, but there were significantly fewer brief arousals (<16 sec) in *rlss* mice (**Figure 5b**). This may reflect once again the state inertia previously described in those mice (Banks et al., 2020), whereby once *rlss* mice have entered a state they tend to remain in that state for longer, hence the lower likelihood of a brief arousal (if the mouse does wake up, then it stays in that state longer as it cannot switch back to NREMS as easily). This hypothesis is further supported by the occurrence of brief awakenings (short arousals ≤16 sec) during NREMS, which is three times less likely in *rlss* mice during undisturbed (baseline) recordings (**Figure 5c**). Of note, the number of muscle twitches in response to the sound was similar across mice ($F(1,7)=0.002$, $p=0.967$, **Figure 5b, right**), indicating no obvious impairment in acute motor or EEG response to environmental triggers (**Figure 5e**).

When looking at the EEG spectra during the sound (8 sec) and during segments of the same length either before or after the sound, we found that – as expected given baseline signatures – there was a significant difference between genotypes. More strikingly, there was a significant Time Point x Genotype interaction if the mouse was in NREMS when the sound occurred ($F(2,14)=5.431$, $p=0.018$), but not if the mouse was in REMS when the sound started ($F(2,14)=1.395$, $p=0.280$) (**Figure 5f**). This indicates that if a sound occurs while a mouse is in NREMS, the evolution of the response in terms of electrophysiological signature from pre- until post-sound epochs is significantly different between WT and *rlss* mice. More specifically, the change in the EEG spectra in response to the sound was more pronounced in WT mice than in *rlss* mice when the mice were originally in NREMS before being woken up.

Thus, *rlss* mice show a conserved arousal threshold, as indicated by the comparable number of full arousals and twitches in both genotypes. Yet, similarly to their response to sleep deprivation, it appears that *rlss* mice show a 'rigidity' in their neuronal dynamics, so that the scope for variation (as measured by spectral power) across states and wake/sleep experiences is markedly reduced.

DISCUSSION

rlss mice are characterized by a mutation in the VAMP2 SNARE protein, that induces a change at the molecular scale by impairing neurotransmitter release (Banks et al., 2020). Here, we found that *rlss* mice display a state inertia, switching less between states, both at behavioural (vigilance state) and at cellular (neuronal) scales. Our results therefore support the idea that sleep regulation is tightly linked to synaptic function. In particular, we show that *rlss* mice display long periods of neuronal silence,

strikingly reminiscent of deep anaesthesia, and which underlie increased SWA during baseline conditions, but lead to an inability to fully adapt neural dynamics in response to behavioural experiences such as sleep deprivation or auditory stimuli. Mathematical modelling revealed that the rate of sleep pressure dissipation is slower in those mice. Finally, we found this neural rigidity is compensated for by global behavioural states, such as increased sleep time in response to sleep deprivation.

An impairment in the 'sleep switch'?

Our previous findings (Banks et al., 2020), combined with the auditory stimulation protocol results described here support the idea of 'vigilance state inertia' in *rlss* mice. The decrease in neurotransmitter release efficiency leads to a difficulty in switching between two consecutive vigilance states in those mice. Previous studies have suggested a mechanism for a sleep/wake switch in both flies and rodents (Pimentel et al., 2016; Saper et al., 2010). 'Flip-flop' switches have been proposed, either to control the transitions between REMS and NREMS (Lu et al., 2006), or to allow rapid transitions between NREMS and wake and prevent animals from lingering between two vigilance states – half awake and half asleep (Saper et al., 2001; Saper et al., 2010). Saper et al. (2001) propose that if neuronal firing is weakened on either side of this bistable switch, then the stability of the switch is compromised; on the other hand, they also propose that the time it takes to transition from one state to the next may depend on the ability for a population of neurons that promote a given state to overcome the 'resistance' of the population of neurons promoting the current state (Saper et al., 2010). In *rlss* mice, we observe an increased stability of each state, both at the behavioural and cellular levels. Concomitantly, we see more similar spectral signatures between vigilance states. This indicates that not only is the sleep-switch not transitioning between states as readily in those mice, but also that it is 'leaky', staying halfway between states, resulting in mixed states with characteristics of both sleep and wake.

Another mouse line (*Sleepy*), developed using a forward genetics approach, exhibited increased NREMS time; the gain-of-function mutation present in these mice affected the *Sik3* gene, and led to a shorter SIK3 protein kinase, which is likely involved in the regulation of sleep amount via its phosphorylation status (Funato et al., 2016). Interestingly, despite this hypersomnia, in contrast to the baseline behavioural phenotype of *rlss* mice, the NREMS delta power was increased in *Sleepy* mice, just like in *rlss* mice. *Sleepy* mice showed an exaggerated response to sleep deprivation, suggesting an increased inherent sleep need despite an increased delta power during baseline wake. The ability of *Sleepy* mice to stay awake when exposed to arousal-promoting stimuli was conserved, showing that, as with *rlss* mice, their ability to be awake should the need arise is not impaired (Funato et al., 2016). But their accumulation of sleep pressure was enhanced leading to longer sleep time when left in undisturbed conditions.

Another mouse model obtained with a forward genetics approach displayed decreased REMS time, with REMS episodes lasting for shorter durations (Funato et al., 2016). The authors thus named those mice *Dreamless* and proposed that the mutation present in this new line (a gain-of-function mutation in the sodium leak channel *Nalcn* gene) led to an increased excitability of REMS-inhibiting neurons. In other words, one could hypothesize that an increase in excitability of REMS-inhibiting neurons would

329 destabilise the sleep-wake switch, leading to more frequent REMS-to-wake/NREMS transitions, and
330 to shorter REMS duration due to the instability of the REMS state.

331 These two other examples, which display some overlapping behavioural phenotypes to the *rlss* mice,
332 do not support the idea that specific genes directly regulate sleep-wake architecture. Rather, those
333 examples back the hypothesis that synaptic function and neuronal excitability – both of which alter
334 the fine balance in neural networks cross-talks – are crucial for sleep-wake regulation.

335 An important point to be discussed, however, is whether the decreased state-transitioning probability
336 observed in *rlss* mice signifies that it is uniformly difficult for them to switch to another state, or rather,
337 that one state is at a stronger disadvantage. In particular, because of the NREMS-like features of wake
338 and REMS in *rlss* mice (e.g. lower power in higher frequencies), it may be less relevant for them to
339 enter full NREMS. We would thus observe an absolute decrease in the probability to enter NREMS
340 relative to other states. And indeed, this is supported by what we observed when looking at state
341 transitioning probabilities from Banks et al. (2020): there is an absolute 44% change in probability to
342 transition between wake and NREMS (wake->NREMS: 34% decrease, NREMS->wake: 10% increase)
343 and a 16% change in probability to transition from REMS to NREMS (REMS->NREMS: 87% decrease,
344 NREMS->REMS: 71% decrease). The REMS->wake transitions are relatively less affected (absolute 8%
345 decrease). This would support the idea that rather than a 'state inertia', those mice revolve around a
346 'default state' mode (Bandarabadi et al., 2020; Buzsáki, 2006; Hinard et al., 2012; Lemieux et al., 2014;
347 Sanchez-Vives et al., 2017; Sanchez-Vives and Mattia, 2014; Timofeev et al., 2020) regardless of their
348 vigilance state, thus making it less relevant to spend time in NREMS.

349

350 **Higher sleep pressure or a higher propensity to return to a 'default state'?**

351 The shorter sleep time in baseline conditions observed in *rlss* mice raises the question of whether
352 these mice have higher sleep efficiency (they can dissipate sleep pressure faster), a decreased sleep
353 pressure build up during waking or that they live under elevated sleep pressure. The two-process
354 model of sleep regulation, which predicts the evolution of Process S, is a useful tool to address this
355 question. A study in humans comparing short sleepers and long sleepers found that both groups had
356 the same constants of increase and decrease of process S, which implied that short sleepers may live
357 under a higher sleep pressure (Aeschbach et al., 1996). Here, we find the *rlss* mice have significantly
358 lower rates of decrease but also a significantly lower upper asymptote of S. These results may
359 therefore indicate than instead of having an inherently elevated sleep pressure (which their lower S
360 upper asymptote argues against), *rlss* mice have a higher propensity to enter or approach the 'default
361 state', due to increased inhibitory tone and/or decreased excitatory tone (induced by the slower
362 neurotransmitter release).

363 There is evidence that the cortical oscillations are not merely an epiphenomenon, or simply a
364 substrate for sleep-related processes to occur (e.g. memory consolidation), but have a role in vigilance
365 state control and sleep regulation (Krone et al., 2021). Thus, if the cortex keeps track of the
366 accumulation of sleep need, then the persistent sleep-like patterns we observe in our cortical
367 recordings could indicate a partial sleep debt discharge across both sleep and waking states.

368

369 **Impaired vesicular release leads to longer neuronal OFF-periods.**

370 Our MUA recordings revealed striking neuronal firing patterns in *rlss* mice during NREMS. Slow-waves
371 were associated with prolonged periods of neuronal silence, where neighbouring neurons stop firing
372 in a coordinated manner for prolonged periods of time, with the longest OFF-periods being about
373 twice as long in *rlss* mice as in WT mice (**Figure 2**). Those periods of neuronal silence resulted in very-
374 low amplitude LFP signals. Such patterns of neuronal activity are seldom seen during natural sleep and
375 are a more common feature of general anaesthesia (Antkowiak, 2002; Lukatch and MacIver, 1996).

376 We have previously described an impairment in vesicular release in *rlss* mice due to the mutation in
377 *Vamp2*, which plays a key role in vesicular and cellular membrane fusion (Banks et al., 2020). *rlss* mice
378 showed a marked decrease in vesicular-release probability following single action potentials. An
379 impairment in vesicular release could lead to a state akin to anaesthesia. Indeed, it has been shown
380 that general anaesthetics, such as isoflurane, propofol or etomidate, induce a decrease in synaptic
381 neurotransmitter release machinery by interacting with multiple SNARE proteins (Herring et al., 2009;
382 Xie et al., 2013). This could account for the long periods of neuronal silence observed in *rlss* mice while
383 they are (naturally) asleep: given their mutation leading to a structural change in VAMP2, which is a
384 SNARE protein, *rlss* mice may present features of an 'inherently anesthetised' state.

385 Interestingly, it was previously shown that injection of the $GABA_A$ agonist muscimol led to a catalepsy-
386 like state, followed by a hyperactive state in mice, with the EEG of both of those states displaying
387 increased power in the slower-frequency range at the expense of the higher-frequency range
388 (Vyazovskiy et al., 2007). This is strikingly similar to our findings, with increased synchrony in all states,
389 and reduced power in high frequencies, alongside a hyperactive phenotype. Furthermore, the
390 dissipation of sleep pressure did not occur under muscimol despite its SWA-enhancing effect, which,
391 the authors conclude, suggests a role for normal physiological sleep in dissipating sleep pressure
392 (Vyazovskiy et al., 2007). Again, this parallels our findings in *rlss* mice which have a markedly reduced
393 constant of decrease of SWA (**Figure 4b**). The authors propose that the effects of muscimol point
394 towards a crucial role for inhibitory connections in slow wave synchronization. Thus, our results
395 suggest that the decreased vesicular release is in many ways akin to increased inhibitory tone and
396 leads to alterations in inhibitory-excitatory balance. The physiological sleep of *rlss* mice is in several
397 ways more similar to non-physiological states such as cataplexy or anaesthesia (e.g. with an
398 inefficiency to properly dissipate sleep pressure) than normal sleep.

399

400 **Switching between anaesthesia and wake**

401 Studies in Drosophila have shown that some 'narrow abdomen' mutants with an altered stability in
402 the switch between wakefulness and sleep displayed increased sensitivity to anaesthesia (Joiner et
403 al., 2013; Krishnan and Nash, 1990). Those mutants present with an altered response to halothane
404 (Krishnan and Nash, 1990) and isoflurane (Joiner et al., 2013): the flies lost consciousness in less time
405 than the WT flies, but were more resistant to the anaesthetic's effects on motor control (Krishnan and
406 Nash, 1990). It was shown that those narrow abdomen mutant flies have altered transitions between
407 wake and anaesthesia, and the authors support the view that the narrow-abdomen gene is part of 4
408 genes necessary for 'neural inertia ', allowing mutual inhibition between arousal-promoting and
409 arousal-suppressing loci, forming a bistable switch between waking and anesthetized states, similar
410 to the sleep switch (Joiner et al., 2013). And indeed, the mutation in those flies affects the orthologue
411 gene to the one affected in the Dreamless mice mentioned above, that present with decreased REMS-

state stability. A later study went on to show that the mutation affecting the narrow-abdomen flies impacts neuronal excitability and firing rates under the control of the circadian clock, and participated in a 'bicycle model' of membrane excitability (Flourakis et al., 2015). This seems to further support the idea discussed above that switching between states requires tightly-regulated excitatory and inhibitory balance between populations of neurons. Also, as mutations with similar effects on neural inertia but opposite effects on anaesthesia induction were observed in flies, it was proposed that the genes (but also possibly brain regions) responsible for anaesthesia induction and state stability are distinct (Joiner et al., 2013). The authors also proposed that the molecular and anatomical pathways involved in sleep homeostasis also contribute to neural inertia (Joiner et al., 2013). This would be in line with our findings, whereby state switching is impaired, and yet, when sleep pressure is high, mice are able to quickly shift to NREMS. Additional evidence suggests that the reversible loss of consciousness caused by anaesthetics occurs via the arousal and sleep pathways, involving both the thalamus and hypothalamus (Franks, 2008), and that the mechanisms underlying sleep homeostasis and anaesthesia overlap (Baker et al., 2014; Gelegen et al., 2018; Pal et al., 2011; Steinberg et al., 2015; Tung et al., 2002).

Yet, these observations start from the premise that sleep and wake are mutually exclusive states between which animals switch in a clear-cut manner, which is now acknowledged to be more complex (Nir and de Lecea, 2023). Indeed, this may not always be the case, as clearly shown by several studies (Bréant et al., 2022; Jang et al., 2022; Vyazovskiy et al., 2007), and states may indeed be viewed on a continuum, with some feature overlap. This is indeed what we see in *rlss* mice with an intrusion of NREMS-like features in REMS and wake states. It is remarkable that the *rlss* mice display only mildly impaired cognitive and behavioural phenotypes typical of wakefulness (Banks et al., 2020), despite the profound alterations in brain activity observed in those mice. Just as the occurrence of slow-waves or decreased neuronal activity which have been previously described in waking and not only in sleep (Fisher et al., 2016; Vanderwolf and Robinson, 1981; Vyazovskiy and Tobler, 2012), our findings further support that vigilance states are not necessarily separate phenomena with unambiguous boundaries, but can share characteristics. Such overlapping features may thus fluctuate depending on specific waking behaviour (Fisher et al., 2016), chemical manipulations (Bréant et al., 2022) or genetic alterations (Funato et al., 2016).

Conclusion

This combination of *in vivo* and computational work provides new insights into the mechanisms that underlie sleep architecture and the alternation between vigilance states, as well as the generation of slow waves. Our results support the idea that synaptic function, and thus neuronal excitability, are direct contributors to sleep-wake architecture. The preserved ability of *rlss* mice to respond to salient external stimuli suggests that neuronal dynamics and sleep-wake architecture can be markedly altered before this leads to a phenotype that would represent an evolutionary disadvantage, with the animal less likely to survive natural selection. Ultimately, our findings regarding the mixed spectral signatures across states in *rlss* mice further support the idea that wake and sleep are not homogeneous states, but rather stand on a continuum of many possible states between full wakefulness and anaesthesia/loss of consciousness.

454

455 METHODS

456 **Animals and housing conditions.**

457 All work was carried out in accordance with the UK Animal [Scientific Procedures] Act 1986 and the
458 University of Oxford's Policy on the Use of Animals in Scientific Research, and in compliance with the
459 Animal Research: Reporting In Vivo Experiments (ARRIVE) guidelines. Mice from the *rlss* colony
460 (MGI:5792085, C3H.Pde6b+ background) were initially obtained from MRC Harwell (U.K.) and were
461 then bred in-house. N=5 *rlss* homozygotes and n=5 WT littermates (all males) were implanted. The
462 experimenter was not blind to the animals' genotype. Over the two months preceding surgeries, to
463 promote weight gain, *rlss* homozygote mice were fed a high-nutrient diet (RM3 diet, ground, Special
464 Diets Services, U.K.) in the form of mash in addition to the regular pellets. Mice were implanted once
465 they had reached a weight nearing or above 30g, which meant that mice were overall 9 weeks older
466 at surgery. The average age and weight of the animals at the time of surgery was 23.8 ± 1.2 weeks &
467 31.9 ± 0.8 g for the homozygotes and 14.7 ± 1.5 weeks & 31.7 ± 1.5 g for the WT mice. Age differences
468 were permitted so that animals were matched by weight. Previous data indicates that this age
469 difference does not contribute to the differences in sleep observed (Banks et al., 2016; McKillop et al.,
470 2018).

471

472 **EEG and laminar probe implantation surgeries**

473 On the day preceding surgery, mice were injected with Dexamethasone (0.2 mg/kg, subcutaneous
474 route). Surgeries were performed using aseptic techniques under isoflurane anaesthesia (1-2%). Mice
475 were provided with meloxicam (5 mg/kg s.c.), buprenorphine (0.1 mg/kg) and Dexamethasone (0.2
476 mg/kg) prior to surgery start. Screws (self-tapping bone screws, stainless steel, length: 4 mm, shaft
477 diameter: 0.85 mm, Fine Science Tools Inc.) were positioned (Motor cortical area (frontal): AP +2 mm,
478 ML +2 mm; Visual cortical area (occipital): AP -3.5 mm, ML + 2.5 mm; Cerebellum: 2 mm behind
479 lambda; Anchor screw: AP -3.5 mm, ML -2.5 mm). Frontal EEG signals are well suited to measure SWA
480 and detect spindles, while occipital EEG signals are better suited to investigate theta activity, active
481 wakefulness and REMS. A small craniotomy was performed around the laminar probe (type A1x16-
482 3mm-100-703-Z16, NeuroNexus Technologies, Ann Arbor, USA) insertion point (≈0.8mm x 0.8 mm,
483 primary motor cortex, AP +1.1, ML -1.75, DV 1.8, tilt of 14°). The tip of the electrode was dyed prior
484 to the surgery with 1,1'-Dioctadecyl-3,3,3',3'-Tetramethylindocarbocyanine Perchlorate dye ('DiI',
485 ThermoFisher Scientific). The probe was grounded to the anchor screw and referenced to the
486 cerebellar screw and carefully lowered into the cortex (1.8 mm from the point at which the tip touches
487 the surface of the brain). Silicon gel (Kwik-Sil, World Precision Instruments, USA) was applied on the
488 craniotomy and the implant cemented. Two electromyography (EMG) electrodes were inserted in the
489 neck muscle and fixed to the back of the head cap with dental cement. Saline was injected
490 subcutaneously (0.1 mL/20 g) to compensate for fluid loss during the duration of the surgery, before
491 placing the mouse in a recovery chamber at 28°C. Animals were administered with Dexamethasone
492 (0.2 mg/kg, s.c.) and meloxicam (5 mg/kg, s.c.) for 1 and 3 days following surgery, respectively.

493

494 **Recordings and Initial Data processing**

Animals were left to recover for at least 2 weeks before being moved to custom-made clear plexiglas cages (20.3 x 32 x 35 cm^3) placed in ventilated, sound-attenuated Faraday chambers (Campden Instruments, UK). Mice were kept in a 12h:12h light-dark cycle (lights on at 9am), with water and food available ad libitum. Temperature within the room was kept at 22±2 °C, with a humidity level of 55±10 %, and light levels of 120-180 lux.

Mice were left to habituate to their new environment for 3 days before being tethered. Recordings were started at least 3 days after tethering, to let the mice habituate to the cables. Signals were recorded using the Multichannel Neurophysiology Recording System (TDT, USA) and the Synapse software (TDT, USA). As described earlier (Banks et al., 2020), EEG and EMG signals were filtered (0.1-100 Hz), amplified (PZ5 NeuroDigitizer preamplifier, Tucker-Davis Technologies) and stored at a sampling rate of 256.9 Hz. Signals were extracted and converted using custom-written Matlab (The MathWorks Inc., USA) scripts as previously described (Guillaumin et al., 2018; McKillop et al., 2018). Vigilance states – wake, NREMS, REMS, or brief awakenings (short arousals ≤16 sec during sleep, as described previously (Vyazovskiy et al., 2009)) – were scored manually using the SleepSign software (Kissei Comtec Co, Nagano, Japan). EEG power density spectra were computed by a Fast Fourier Transform (Hanning window; 0.25-Hz resolution). More detailed recording and initial analysis methods were as published (Banks et al., 2016; Banks et al., 2020; McKillop et al., 2018). As the focus of the present study was on the slower frequencies, spectra only show power for frequencies up to 20 Hz.

Sleep deprivation

Sleep deprivation (SD) was performed for 6 consecutive hours starting from light onset (ZT0). Animals were kept awake by providing them with new objects to explore. If the mice were getting drowsy, nesting material was taken away from the cage temporarily. SD was successful as only 7.8 ± 1.7 minutes (mean ± SEM) of sleep were detected during the 6 h of SD. Following sleep deprivation, mice were left undisturbed for at least 18 h.

Auditory stimulation

Sounds of 8kHz, 75dB were played for 8 sec every minute during 1h30 (90 repetitions of 8-sec sound, 52-sec silence). This 1h30 session was performed 4 times across 24 h: ZT 0.5 – 2; ZT 7.5 – 9; ZT 12.5 – 14; ZT 20 – 21.5. Speakers were placed 70 cm above each animal, within the Faraday sound-attenuated chambers.

Detection of OFF-periods

Detection of low-amplitude neural activity segments ('OFF-periods') was performed using the GUI made available by C.Harding, described in Harding et al. (2023). Default parameters of the GUI were used for OFF-period detection (Calinski-Harabaz clustering evaluation method; Clustering variable 1: amplitude, 15 smoothing points; clustering variable 2: amplitude, 5 smoothing points; clustering sample size: 1%). Out of the 16 channels, 5-10 MUA channels (and corresponding LFP channel for visualization) were selected for each mouse, selecting only those that were stable across a 48h (baseline day + sleep deprivation day). The first 12 h of the baseline day were used as a new dataset

536 against which the detection parameters were calculated for each mouse. The parameters ('pre-sets')
537 were then re-used to detect OFF-periods for the next 36 h of recording.

538 In some instances (specified in the legends and text), only the 5% longest OFF-periods were included.
539 The 5% threshold was chosen to include enough OFF-periods, while still focusing on the longest ones,
540 wherever that was the focus of our investigations.

541

542 **Application of the 'elaborated two-process model'**

543 The estimation and optimisation of the model parameters (gain constant gc, describing the decay rate
544 of SWA; rise constant rs and upper asymptote S_U) were performed exactly as described in Guillaumin
545 et al. (2018), using SWA calculated across a 24-h baseline day and a sleep deprivation day (6-h sleep
546 deprivation + 18-h recovery sleep). For the baseline-only optimisations, the baseline recordings were
547 artificially duplicated for the estimation/optimisation of the parameters, as described in the above-
548 mentioned publication. For the BL+SD day, the 24-h baseline day followed by the sleep deprivation
549 day were used.

550

551 **Perfusions and micro-lesions**

552 Mice were injected with Pentobarbital (200mg in 1 mL, i.p. injection of 0.01mL/g body weight).
553 Microlesions of 3 selected channels on the laminar probe were then performed using a NanoZ device
554 (White Matter) before the mice were transcardially perfused with a PBS solution, followed by
555 paraformaldehyde (PFA, 4% in PBS). Brains were removed and placed in PFA (4% in PBS) for 48 h,
556 after which they were transferred to a 30% sucrose solution (in PBS) for cryoprotection. Once sunk to
557 the bottom of the vial, brains were briefly rinsed in PBS and embedded in O.C.T. compound and frozen
558 at -80°C until cutting.

559

560 **Histology**

561 To confirm electrode placement, slices were prepared using a cryostat (Cryotome FSE,
562 ThermoScientific; -22°C, 50µm-thick sections) and mounted on glass slides. Slides were subsequently
563 mounted under cover glasses with ProLong Glass Antifade mountant with NucBlue stain
564 (ThermoFisher Scientific). Sections were digitized using an LSM 710 laser scanning confocal
565 microscope and ZEN image acquisition software (Zeiss) (**Figure S3**).

566

567 **Statistical analysis**

568 All statistical analyses were performed using SPSS (IBM Corp., Release 23.0.0.2) and Matlab (The
569 MathWorks Inc., USA). The nature of the tests used and corresponding results are reported within
570 figure legends or within the main text of the Results section. Wilcoxon rank sum test was used where
571 normality was not observed (Kolmogorov Smirnov test).

572

573 **Acknowledgements**

We thank Prof. Peter Achermann for advice on Process S simulations and Prof. Irene Tracey for stimulating discussions and valuable suggestions regarding data interpretation. We also thank Dr Laura E. McKillop for valuable advice on surgical procedures. M.C.C.G. was supported by a BBSRC DTP grant (BB/J014427/1), a Swiss National Science Foundation grant (no. 310030_189110) and a Clarendon Fund Scholarship from the University of Oxford. C.D.H. was supported by funding from the Engineering and Physical Sciences Research Council (EPSRC, EP/S515541/1). L.B.K. was supported by a Wellcome Trust PhD studentship (203971/Z/16/Z) and by a Mann Senior Scholarship in medical sciences at Hertford College, Oxford. T.Y. was supported by the Naito Foundation (Grant for Studying Overseas), a Uehara Memorial Foundation (Postdoctoral Fellowships for Research Abroad) and a Wellcome Trust Senior Investigator Award (106174/Z/14/Z). M.C.K. was supported by a Berrow Foundation Lord Florey Scholarship. C.B.-D. was supported by a Wellcome Trust PhD studentship (109059/Z/15/Z) and a Clarendon Fund Scholarship from the University of Oxford. P.M.N. was supported by the MRC (grant codes MC_U142684173 and MC_UP_1503/2). S.N.P. was funded by the BBSRC (BB/ I021086/1) and a Wellcome Trust Strategic Award (098461/Z/12/Z). V.V.V. was funded by a John Fell OUP Research Fund Grant (131/032), a Wellcome Trust Strategic Award (098461/Z/12/Z) and by Medical Research Council (UK) Grant MR/S01134X/1.

Author contributions

MCCG: implantation surgeries, experiments and data collection, data analysis, writing of the manuscript and figures, funding support.

CH developed the OFF-period detection algorithm.

LBK contributed to the development of the OFF-period detection algorithm and advised on implantation, microlesions and histology.

TY advised on surgeries and auditory stimulation protocol.

MCK advised on technical issues.

CBD advised on methodology and data analysis for the auditory stimulation experiment.

GTB and PN assisted in the development of the mouse model and initial phenotyping of the *rlss* mice.

SNP advised on study design, methodology, supervision, funding support.

VVV: conceptualisation/study design, methodology, supervision, direction of data analysis and manuscript preparation, funding support.

606 MAIN FIGURE PANELS

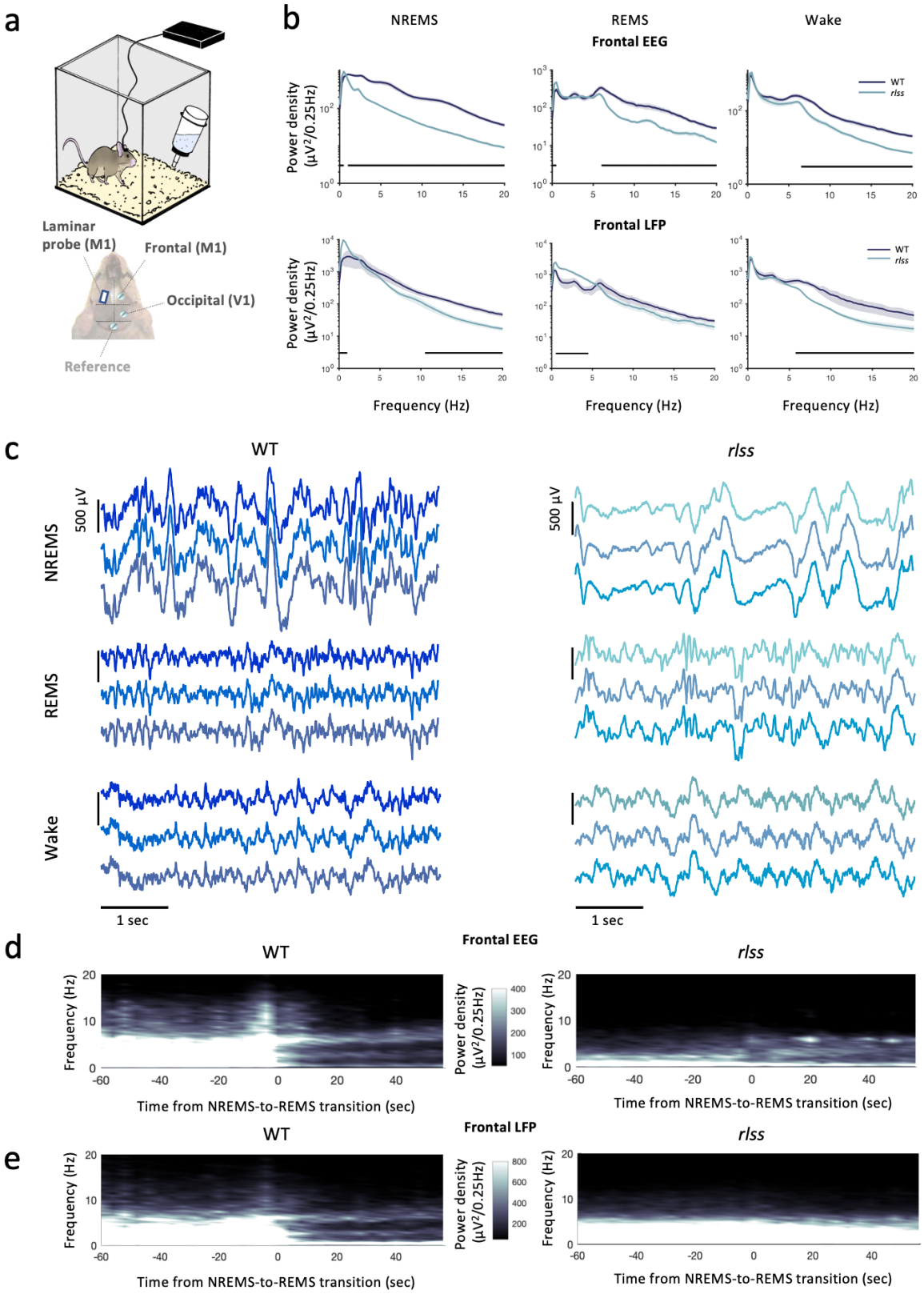

607

608 **Figure 1. *rlss* mice show an increased level of similarity between vigilance state signatures.**

609 a) Schematic of recording set up. M1: primary motor cortex; V1: primary visual cortex.

b) Frontal EEG (upper panels) and LFP (lower panels) power spectra during NREMS, REMS and wake in WT and *rlss* mice. Black bars at the bottom indicate the frequency bins for which the power is significantly different ($p<0.05$) between WT and *rlss* mice. Values shown as mean ± SEM.

c) Examples of three LFP traces from a WT mouse (left) and *rlss* mouse (right) during NREMS, REMS and wake.

d) Evolution of the power spectra in the frontal EEG at NREMS-to-REMS transitions averaged across WT (left) and *rlss* (right) mice.

e) As in d), but for LFP signals. Note that here n(WT)=3.

Unless otherwise stated, n(WT)=5 and n(*rlss*)=5.

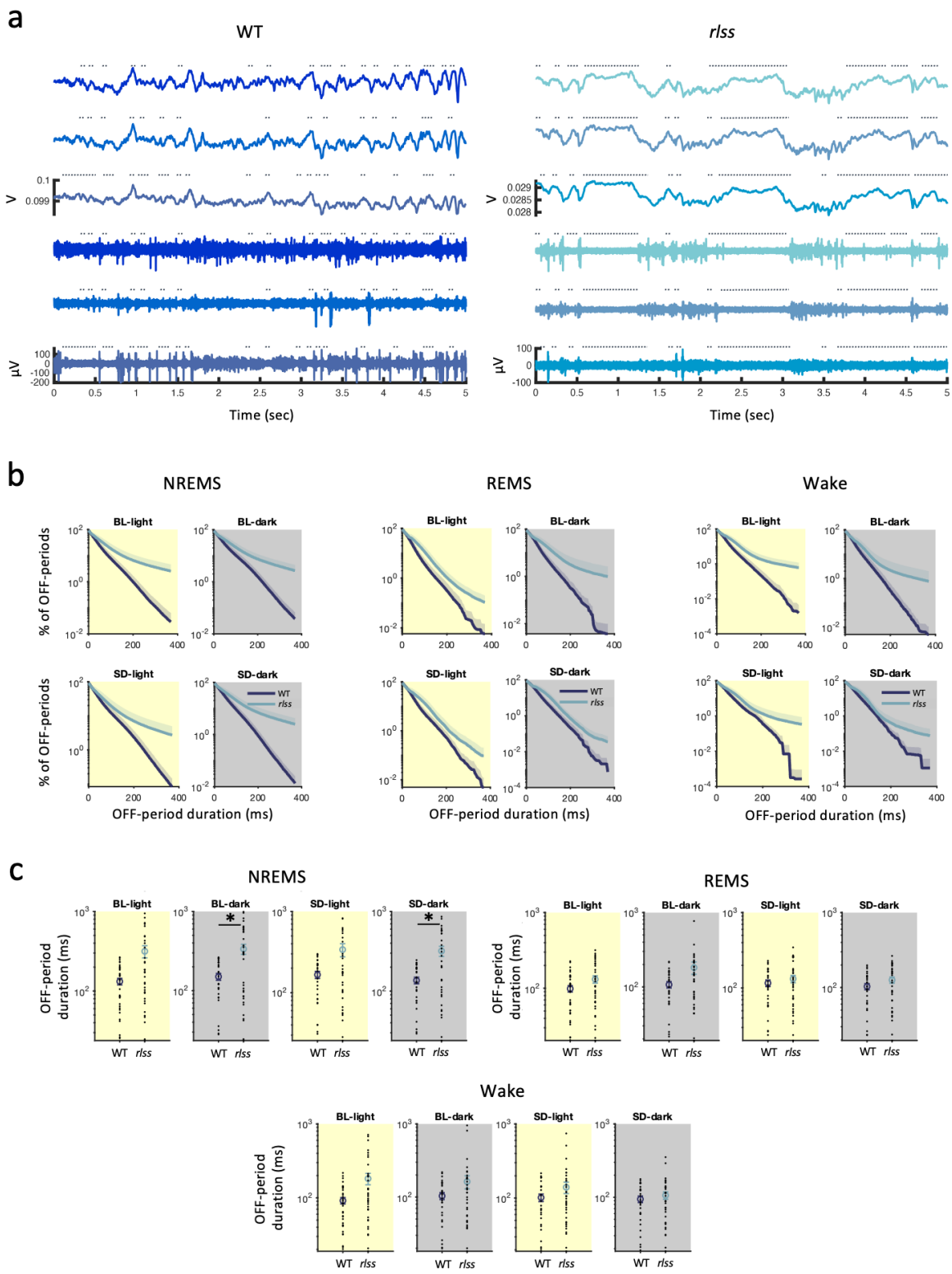

Figure 2. *rlss* mice show prolonged periods of neuronal silence across vigilance states that are reminiscent of burst suppression patterns.

a) Examples of three LFP (upper traces) and corresponding MUA (lower traces) signals in a WT mouse (left) and *rlss* mouse (right) during 5 sec of NREMS. Dotted lines indicate location of OFF-periods as detected by the algorithm (see Methods) with no threshold applied.

b) Survival curves of OFF-periods (relative to their duration) in NREMS (left), REMS (middle) and wake (right) during a baseline (BL) day (upper panels) and a SD day (lower panels), separately for the light and dark phases of a 24-h day in WT and *rlss* mice. Values shown as mean + SEM.

c) Average OFF-period durations of the 5% longest OFF-periods during NREMS (upper panels), REMS (middle) and wake (lower panels), in a BL (left) or SD day (right) separately for the light and dark phases. Values shown as mean ± SEM, with black dots indicating individual channels. Wilcoxon rank sum test; * indicates $p<0.05$, ** $p<0.01$, *** $p<0.001$.

n(WT), n(*rlss*)=5. BL: baseline, SD: sleep deprivation.

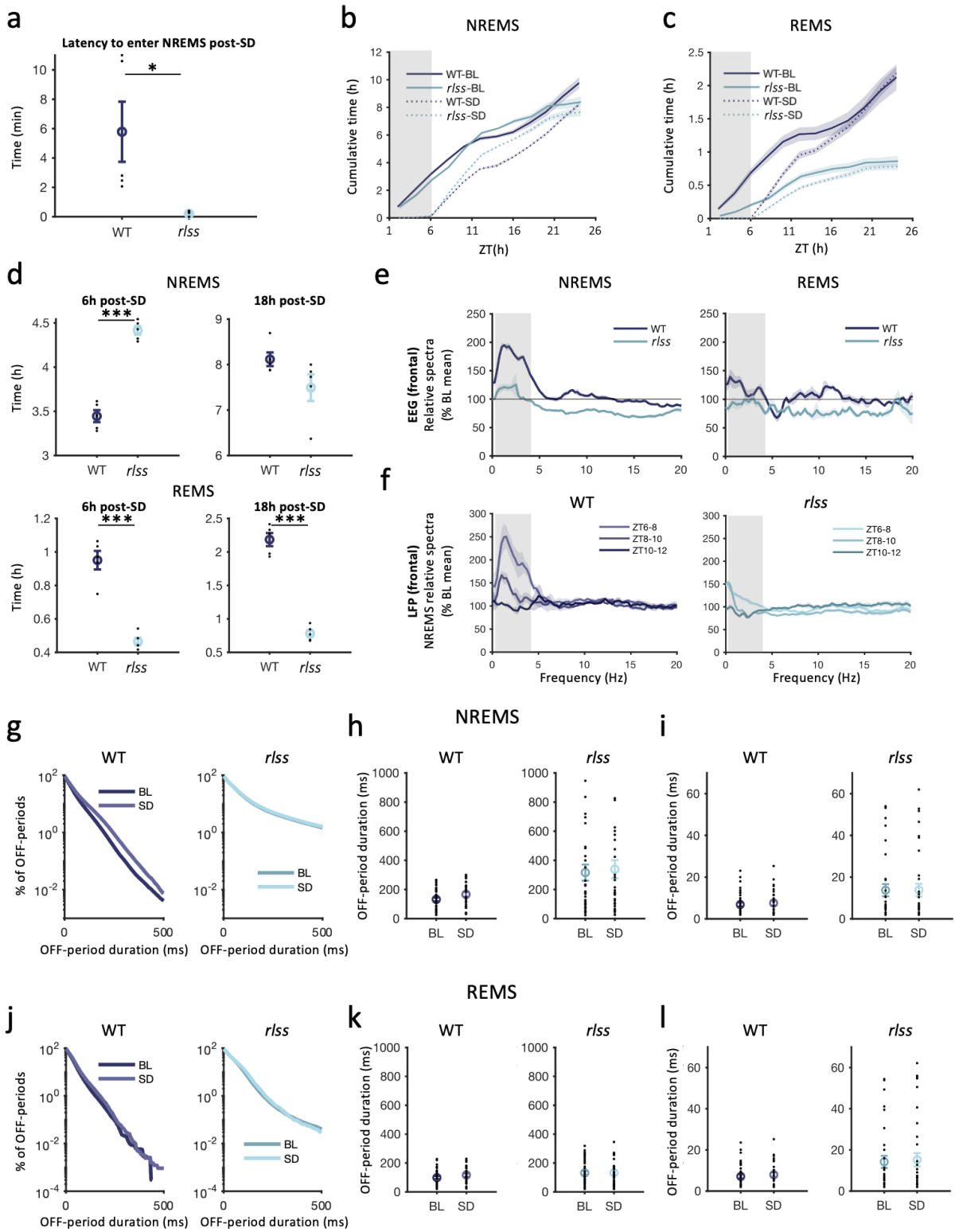

Figure 3. Response to sleep deprivation reveals a decreased sleep quality that is compensated for by an increase in sleep quantity in *rlss* mice.

a) Latency to enter NREMS following a 6-h sleep deprivation (SD) protocol.

b) Cumulative time spent (in 2-h bins) in NREMS in WT and *rlss* mice during a baseline (BL) or a SD day. Highlighted in grey is the SD period for the SD day only.

c) As in b) for REMS.

641 d) Amount of time spent in NREMS (top panels) or REMS (bottom panels) during the 6h (left panels) or 18h
642 (right panels) following a 6-h SD protocol in WT and *rlss* mice.

643 e) Frontal EEG spectra in NREMS (left) and REMS (right) relative to the baseline mean in WT and *rlss* during
644 the 2h following a 6-h SD protocol. Delta frequency band (0.5-4 Hz) highlighted in grey.

645 f) LFP spectra in NREMS relative to baseline mean in WT (left) and *rlss* (right) mice in the 6h following a 6-h
646 SD protocol, separated in 2-h blocs. Delta frequency band (0.5-4 Hz) highlighted in grey.

647 g) Survival curves of OFF-periods (relative to their duration) occurring during NREMS during the light phase
648 of a BL and SD day in WT (left) and *rlss* (right) mice.

649 h) Average OFF-period duration of the 5% longest OFF-periods in NREMS in the light phase of a BL and SD
650 day in WT (left) and *rlss* (right) mice. Black dots indicate individual channels.

651 i) As in h) but for the 5% shortest OFF-periods.

652 j) As in g), but for OFF-periods occurring during REMS.

653 k) As in h), but for OFF-periods occurring during REMS.

654 l) As in i), but for OFF-periods occurring during REMS.

655 Values shown as mean ± SEM, with black dots indicated individual values (mice in a & d, or channels in h, i, k &
656 l). n(WT)=5 (3 for LFP-derived parameters), n(*rlss*)=5. Independent samples t-tests in a) and d); * indicates
657 $p<0.05$, ***$p<0.001$. BL: baseline, SD: sleep deprivation, ZT: zeitgeber time.

658

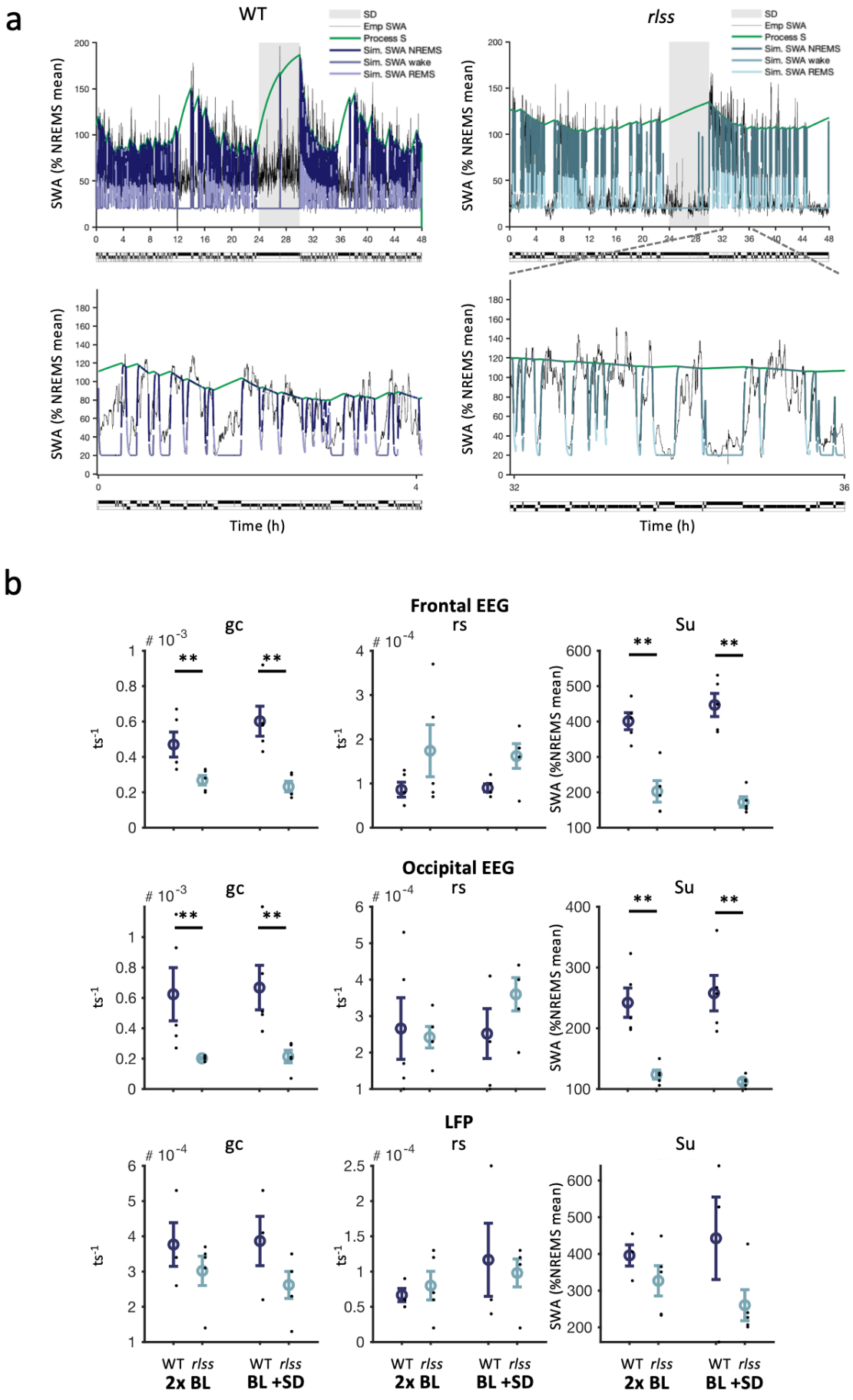
a
WT
rlss
SD
Emp SWA
Process S
Sim. SWA NREMS
Sim. SWA wake
Sim. SWA REMS
SWA (% NREMS mean)
Time (h)
b
Frontal EEG
Occipital EEG
LFP
gc
rs
Su
ts-1
SWA (%NREMS mean)
WT rlss
2x BL
BL +SD

659

Figure 4. Sleep homeostasis dynamics are altered in *rlss* mice, with a lower decay rate of sleep pressure.

a) Upper panels: Example of empirical and simulated slow-wave activity (SWA) across 48 h (24 h of baseline + 6-h sleep-deprivation + 18-h recovery) in an example WT (left) and *rlss* (right) mouse. Lower panels: zoomed-in inserts of a 4-hour section from the corresponding upper panels. Colours indicate the corresponding vigilance state, also shown underneath each panel as a hypnogram.

b) Model parameters when modelling the SWA levels of the frontal EEG signal (upper panels), occipital EEG (middle panels) and LFP (lower panels), using 2 BL days (left panels of each parameter) or a BL+SD day (right panels of each parameter), in WT (n=5 for EEG, n=3 for LFP) and *rlss* mice (n=5). Values shown as mean ± SEM; black dots indicate individual values. Non-parametric Mann Whitney tests; ** $p<0.01$.

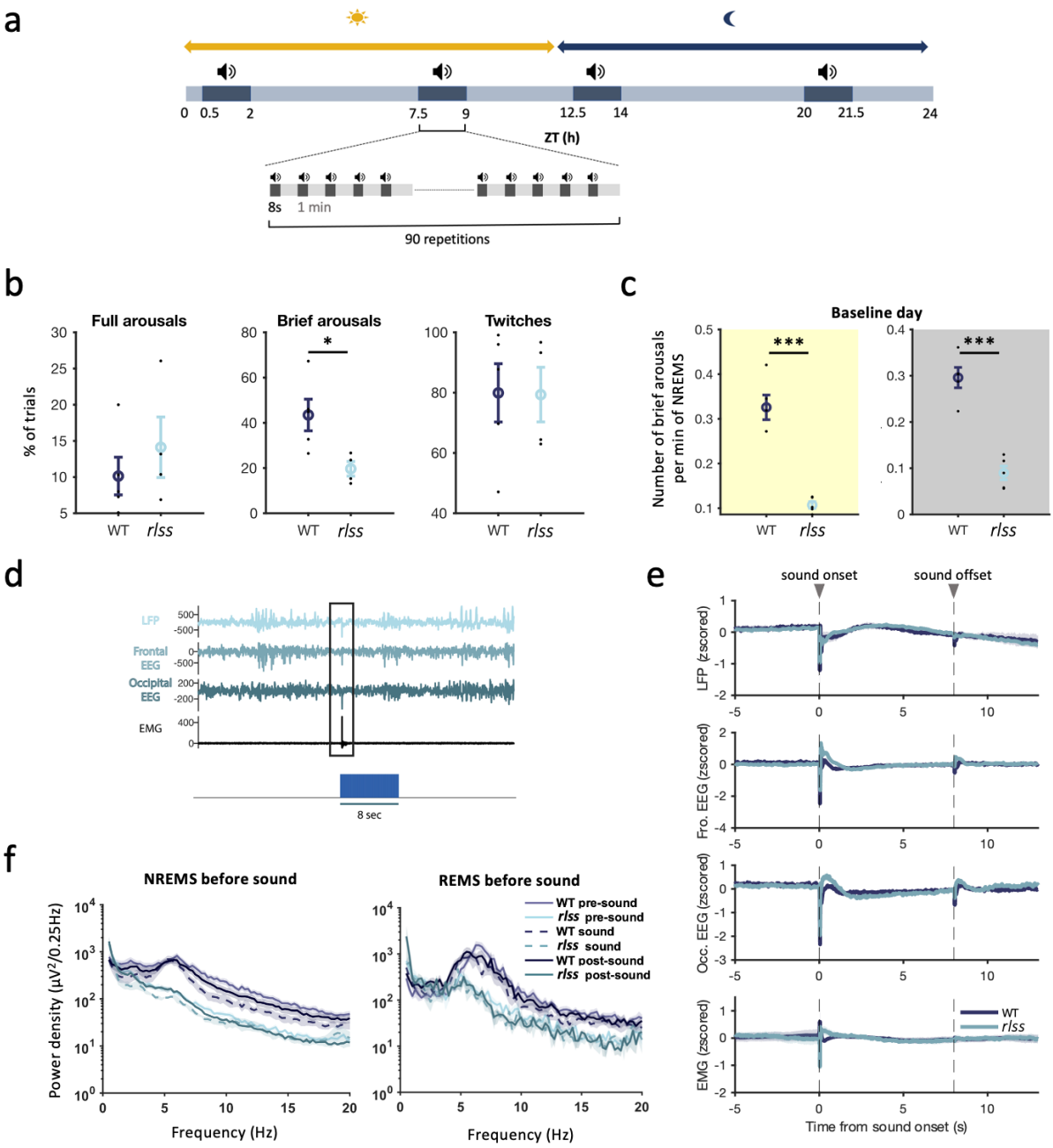

Figure 5. *rlss* mice show a conserved arousal threshold but an impaired neuronal response to an aurditory stimulus during sleep.

a) Schematic of experimental design.

b) Number of full arousals, brief arousals and muscle twitches in response to a sound.

c) Number of brief arousals per min of NREMS during the light and the dark phase of a baseline day.

d) Example of a muscle twitch and associated artifacts in the LFP and EEG channels in response to a sound.

e) LFP (1 representative channel per mouse), frontal EEG, occipital EEG and EMG around sounds. Signals are extracted from all sound trials occurring during the light phase, and z-scored before being averaged across trials and across mice.

f) Power density spectra calculated from the occipital EEG in the 8 sec before, 8 sec during and 8 sec after a sound, if the sound onset occurred during NREMS (left) or REMS (right).

686 n(WT)=5 (3 for LFP), n(*rlss*)=4. Values shown as mean ± SEM; black dots indicate individual values.
687 Independent samples t-tests; *p<0.05, ***p<0.001. Occ.: occipital, ZT: zeitgeber time.

688

689

690 SUPPLEMENTARY FIGURE PANELS
691

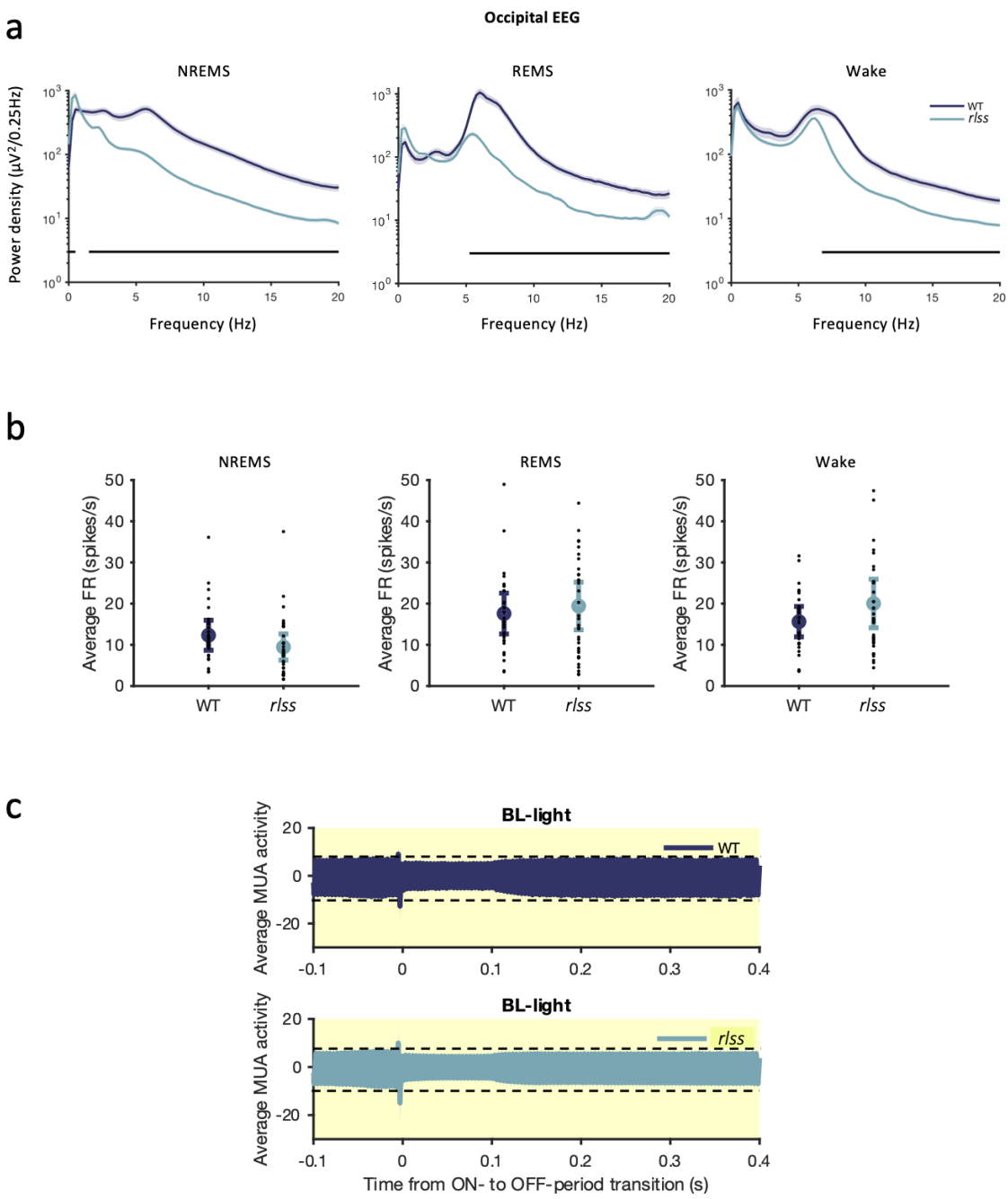

692

693 **Figure S1.**

694 a) Occipital EEG power spectra during NREMS, REMS and Wake in WT and *rlss* mice. Black bars at the
695 bottom indicate the frequency bins for which the power is significantly different ($p<0.05$) between WT
696 and *rlss* mice.

697 b) Average firing rate (FR, calculated from the multi-unit activity (MUA) as number of spikes per second)
698 in each vigilance state, calculated from the light phase of a baseline day. n(WT)=4, n(*rlss*)=5.
699

700 c) Average multi-unit activity across channels at ON- to OFF-period transitions in WT mice (top) and *rlss*
701 mice (bottom). Only transitions during a 12-h light phase of a baseline day is included and only
702 transition to OFF-periods that last at least 100 ms were considered here.

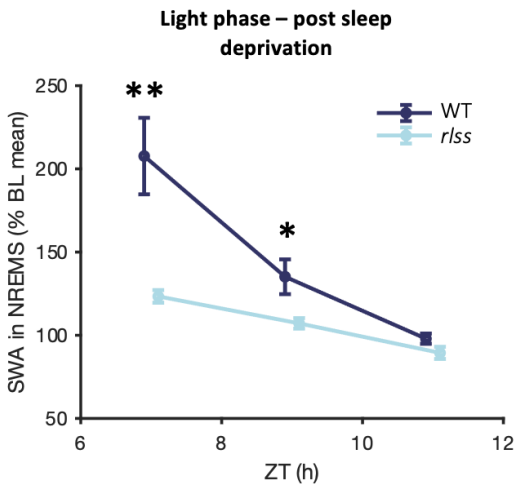

703
704
705 **Figure S2.** SWA levels during NREMS, from LFP recordings, in the 6 h following 6 h of sleep deprivation.
706 Values normalised against a 24-h baseline mean, plotted in 2-h bins. Mean ± SEM; n(WT)=3, n(Hom)=5.
707 Two-way ANOVA revealed a main effect of Time Point ($F(2,12)=80.604$, $p<0.001$), Genotype
708 ($F(1,6)=17.313$, $p=0.006$), and a significant interaction Time Point* Genotype ($F(2,12)=23.745$, $p<0.001$).
709 Post-hoc testing with Bonferroni correction for multiple comparisons are indicated on the plot. *
710 $p<0.05$, **$p<0.01$. BL: baseline, SWA: slow-wave activity, ZT: zeitgeber time.
711

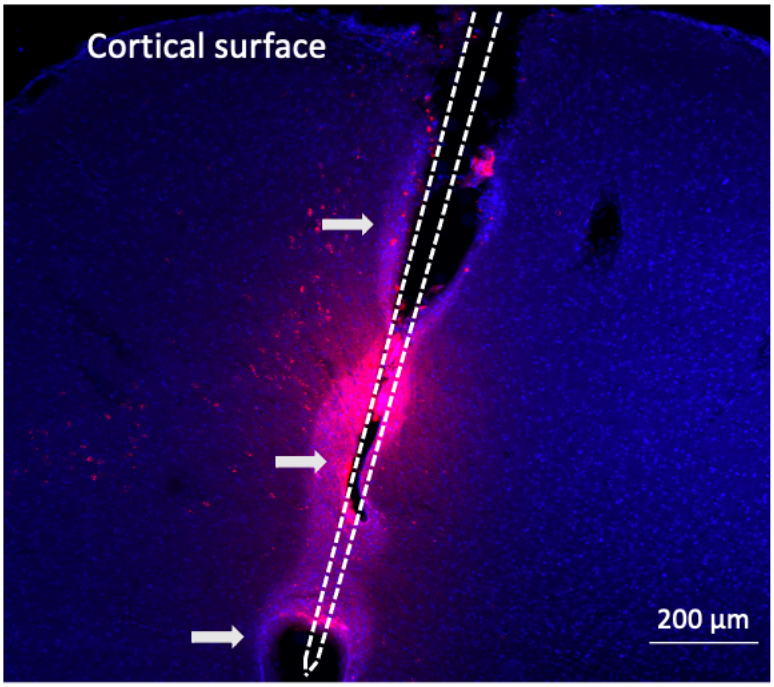

Figure S3. Confocal image of laminar probe placement from one mouse. Grey arrows indicate micro-lesioning sites (see Methods). DiI reported in pink. Cell nuclei in blue (NucBlue).

720

721 REFERENCES

722

723 Achermann, P., and Borbely, A.A. (2003). Mathematical models of sleep regulation. Front
724 Biosci *8*, s683-693.

725 Achermann, P., Dijk, D.J., Brunner, D.P., and Borbely, A.A. (1993). A model of human sleep
726 homeostasis based on EEG slow-wave activity: quantitative comparison of data and
727 simulations. Brain Res Bull *31*, 97-113.

728 Aeschbach, D., Cajochen, C., Landolt, H., and Borbely, A.A. (1996). Homeostatic sleep
729 regulation in habitual short sleepers and long sleepers. Am J Physiol *270*, R41-53.

730 Antkowiak, B. (2002). In vitro networks: cortical mechanisms of anaesthetic action. Br J
731 Anaesth *89*, 102-111.

732 Baker, R., Gent, T.C., Yang, Q., Parker, S., Vyssotski, A.L., Wisden, W., Brickley, S.G., and Franks,
733 N.P. (2014). Altered activity in the central medial thalamus precedes changes in the neocortex
734 during transitions into both sleep and propofol anesthesia. J Neurosci *34*, 13326-13335.

735 Bandarabadi, M., Vassalli, A., and Tafti, M. (2020). Sleep as a default state of cortical and
736 subcortical networks. Current Opinion in Physiology *15*, 60-67.

737 Banks, G., Nolan, P.M., and Peirson, S.N. (2016). Reciprocal interactions between circadian
738 clocks and aging. Mamm Genome *27*, 332-340.

739 Banks, G.T., Guillaumin, M.C.C., Heise, I., Lau, P., Yin, M., Bourbia, N., Aguilar, C., Bowl, M.R.,
740 Esapa, C., Brown, L.A.*, et al.* (2020). Forward genetics identifies a novel sleep mutant with
741 sleep state inertia and REM sleep deficits. Sci Adv *6*, eabb3567.

742 Borbely, A.A., Baumann, F., Brandeis, D., Strauch, I., and Lehmann, D. (1981). Sleep
743 deprivation: effect on sleep stages and EEG power density in man. Electroencephalogr Clin
744 Neurophysiol *51*, 483-495.

745 Borbely, A.A., Tobler, I., and Hanagasioglu, M. (1984). Effect of sleep deprivation on sleep and
746 EEG power spectra in the rat. Behav Brain Res *14*, 171-182.

747 Bréant, B.J., Mengual, J.P., Bannerman, D.M., Sharp, T., and Vyazovskiy, V.V. (2022).
748 "Paradoxical wakefulness" induced by psychedelic 5-methoxy-N,N-dimethyltryptamine in
749 mice. BioRxiv.

750 Brown, E.N., Lydic, R., and Schiff, N.D. (2010). General anesthesia, sleep, and coma. N Engl J
751 Med *363*, 2638-2650.

752 Buzsáki, G. (2006). The Brain's Default State: Self-Organized Oscillations in Rest and Sleep. In
753 Rhythms of the Brain (New York: Oxford Academic).

754 Calvet, J., Fourment, A., and Thiefry, M. (1973). Electrical activity in neocortical projection and
755 association areas during slow wave sleep. Brain Res *52*, 173-187.

756 Clark, D.L., and Rosner, B.S. (1973). Neurophysiologic effects of general anesthetics. I. The
757 electroencephalogram and sensory evoked responses in man. Anesthesiology *38*, 564-582.

758 Contreras, D., and Steriade, M. (1995). Cellular basis of EEG slow rhythms: a study of dynamic
759 corticothalamic relationships. J Neurosci *15*, 604-622.

760 Dijk, D.J., Beersma, D.G., and Daan, S. (1987). EEG power density during nap sleep: reflection
761 of an hourglass measuring the duration of prior wakefulness. J Biol Rhythms *2*, 207-219.

762 Fisher, S.P., Cui, N., McKillop, L.E., Gemignani, J., Bannerman, D.M., Oliver, P.L., Peirson, S.N.,
763 and Vyazovskiy, V.V. (2016). Stereotypic wheel running decreases cortical activity in mice. Nat
764 Commun *7*, 13138.

765 Flourakis, M., Kula-Eversole, E., Hutchison, A.L., Han, T.H., Aranda, K., Moose, D.L., White,
766 K.P., Dinner, A.R., Lear, B.C., Ren, D.J.*, et al.* (2015). A Conserved Bicycle Model for Circadian
767 Clock Control of Membrane Excitability. Cell *162*, 836-848.

768 Franks, N.P. (2008). General anaesthesia: From molecular targets to neuronal pathways of
769 sleep and arousal. Nature Reviews Neuroscience *9*, 370-386.

770 Funato, H., Miyoshi, C., Fujiyama, T., Kanda, T., Sato, M., Wang, Z., Ma, J., Nakane, S., Tomita,
771 J., Ikkyu, A.*, et al.* (2016). Forward-genetics analysis of sleep in randomly mutagenized mice.
772 Nature *539*, 378-383.

773 Gelegen, C., Miracca, G., Ran, M.Z., Harding, E.C., Ye, Z., Yu, X., Tossell, K., Houston, C.M.,
774 Yustos, R., Hawkins, E.D.*, et al.* (2018). Excitatory Pathways from the Lateral Habenula Enable
775 Propofol-Induced Sedation. Curr Biol *28*, 580-587 e585.

776 Guillaumin, M.C.C., McKillop, L.E., Cui, N., Fisher, S.P., Foster, R.G., de Vos, M., Peirson, S.N.,
777 Achermann, P., and Vyazovskiy, V.V. (2018). Cortical region-specific sleep homeostasis in
778 mice: effects of time of day and waking experience. Sleep *41*.

779 Harding, C.D., Guillaumin, M.C.C., Krone, L.B., Kahn, M.C., Blanco-Duque, C., Mikutta, C., and
780 Vyazovskiy, V.V. (2023). Detection of neuronal OFF periods as low amplitude neural activity
781 segments. BMC Neurosci *24*, 13.

782 Hayat, H., Marmelshtein, A., Krom, A.J., Sela, Y., Tankus, A., Strauss, I., Fahoum, F., Fried, I.,
783 and Nir, Y. (2022). Reduced neural feedback signaling despite robust neuron and gamma
784 auditory responses during human sleep. Nat Neurosci *25*, 935-943.

785 Herring, B.E., Xie, Z., Marks, J., and Fox, A.P. (2009). Isoflurane inhibits the neurotransmitter
786 release machinery. J Neurophysiol *102*, 1265-1273.

787 Hinard, V., Mikhail, C., Pradervand, S., Curie, T., Houtkooper, R.H., Auwerx, J., Franken, P., and
788 Tafti, M. (2012). Key electrophysiological, molecular, and metabolic signatures of sleep and
789 wakefulness revealed in primary cortical cultures. J Neurosci *32*, 12506-12517.

790 Huang, Y.G., Flaherty, S.J., Pothecary, C.A., Foster, R.G., Peirson, S.N., and Vyazovskiy, V.V.
791 (2021). The relationship between fasting-induced torpor, sleep, and wakefulness in
792 laboratory mice. Sleep *44*.

793 Jang, R.S., Ciliberti, D., Mankin, E.A., and Poe, G.R. (2022). Recurrent Hippocampo-neocortical
794 sleep-state divergence in humans. Proc Natl Acad Sci U S A *119*, e2123427119.

795 Joiner, W.J., Friedman, E.B., Hung, H.T., Koh, K., Sowcik, M., Sehgal, A., and Kelz, M.B. (2013).
796 Genetic and Anatomical Basis of the Barrier Separating Wakefulness and Anesthetic-Induced
797 Unresponsiveness. Plos Genet *9*.

798 Krishnan, K.S., and Nash, H.A. (1990). A Genetic-Study of the Anesthetic Response - Mutants
799 of Drosophila-Melanogaster Altered in Sensitivity to Halothane. P Natl Acad Sci USA *87*, 8632-
800 8636.

801 Krone, L.B., Yamagata, T., Blanco-Duque, C., Guillaumin, M.C.C., Kahn, M.C., van der Vinne,
802 V., McKillop, L.E., Tam, S.K.E., Peirson, S.N., Akerman, C.J*., et al.* (2021). A role for the cortex
803 in sleep-wake regulation. Nat Neurosci *24*, 1210-1215.

804 Lemieux, M., Chen, J.Y., Lonjers, P., Bazhenov, M., and Timofeev, I. (2014). The impact of
805 cortical deafferentation on the neocortical slow oscillation. J Neurosci *34*, 5689-5703.

806 Lu, J., Sherman, D., Devor, M., and Saper, C.B. (2006). A putative flip-flop switch for control of
807 REM sleep. Nature *441*, 589-594.

808 Lukatch, H.S., and MacIver, M.B. (1996). Synaptic mechanisms of thiopental-induced
809 alterations in synchronized cortical activity. Anesthesiology *84*, 1425-1434.

810 Massimini, M., Huber, R., Ferrarelli, F., Hill, S., and Tononi, G. (2004). The sleep slow oscillation
811 as a traveling wave. J Neurosci *24*, 6862-6870.

McKillop, L.E., Fisher, S.P., Cui, N.Y., Peirson, S.N., Foster, R.G., Wafford, K.A., and Vyazovskiy, V.V. (2018). Effects of Aging on Cortical Neural Dynamics and Local Sleep Homeostasis in Mice. J Neurosci *38*, 3911-3928.

Mukovski, M., Chauvette, S., Timofeev, I., and Volgushev, M. (2007). Detection of active and silent states in neocortical neurons from the field potential signal during slow-wave sleep. Cereb Cortex *17*, 400-414.

Neckelmann, D., and Ursin, R. (1993). Sleep stages and EEG power spectrum in relation to acoustical stimulus arousal threshold in the rat. Sleep *16*, 467-477.

Nir, Y., and de Lecea, L. (2023). Sleep and vigilance states: Embracing spatiotemporal dynamics. Neuron.

Nir, Y., Vyazovskiy, V.V., Cirelli, C., Banks, M.I., and Tononi, G. (2015). Auditory responses and stimulus-specific adaptation in rat auditory cortex are preserved across NREM and REM sleep. Cereb Cortex *25*, 1362-1378.

Pal, D., Lipinski, W.J., Walker, A.J., Turner, A.M., and Mashour, G.A. (2011). State-specific Effects of Sevoflurane Anesthesia on Sleep Homeostasis Selective Recovery of Slow Wave but Not Rapid Eye Movement Sleep. Anesthesiology *114*, 302-310.

Pimentel, D., Donlea, J.M., Talbot, C.B., Song, S.M., Thurston, A.J.F., and Miesenbock, G. (2016). Operation of a homeostatic sleep switch. Nature *536*, 333-337.

Rechtschaffen, A., Hauri, P., and Zeitlin, M. (1966). Auditory awakening thresholds in REM and NREM sleep stages. Percept Mot Skills *22*, 927-942.

Sanchez-Vives, M.V., Massimini, M., and Mattia, M. (2017). Shaping the Default Activity Pattern of the Cortical Network. Neuron *94*, 993-1001.

Sanchez-Vives, M.V., and Mattia, M. (2014). Slow wave activity as the default mode of the cerebral cortex. Arch Ital Biol *152*, 147-155.

Saper, C.B., Chou, T.C., and Scammell, T.E. (2001). The sleep switch: hypothalamic control of sleep and wakefulness. Trends Neurosci *24*, 726-731.

Saper, C.B., Fuller, P.M., Pedersen, N.P., Lu, J., and Scammell, T.E. (2010). Sleep state switching. Neuron *68*, 1023-1042.

Shanker, A., Abel, J.H., Schamberg, G., and Brown, E.N. (2021). Etiology of Burst Suppression EEG Patterns. Front Psychol *12*, 673529.

842 Steinberg, E.A., Wafford, K.A., Brickley, S.G., Franks, N.P., and Wisden, W. (2015). The role of
843 K(2)p channels in anaesthesia and sleep. Pflugers Arch *467*, 907-916.

844 Steriade, M., McCormick, D.A., and Sejnowski, T.J. (1993). Thalamocortical oscillations in the
845 sleeping and aroused brain. Science *262*, 679-685.

846 Steriade, M., Timofeev, I., and Grenier, F. (2001). Natural waking and sleep states: a view from
847 inside neocortical neurons. J Neurophysiol *85*, 1969-1985.

848 Thomas, C.W., Guillaumin, M.C., McKillop, L.E., Achermann, P., and Vyazovskiy, V.V. (2020).
849 Global sleep homeostasis reflects temporally and spatially integrated local cortical neuronal
850 activity. Elife *9*.

851 Timofeev, I., Schoch, S.F., LeBourgeois, M.K., Huber, R., Riedner, B.A., and Kurth, S. (2020).
852 Spatio-temporal properties of sleep slow waves and implications for development. Curr Opin
853 Physiol *15*, 172-182.

854 Tung, A., Szafran, M.J., Bluhm, B., and Mendelson, W.B. (2002). Sleep deprivation potentiates
855 the onset and duration of loss of righting reflex induced by propofol and isoflurane.
856 Anesthesiology *97*, 906-911.

857 Vanderwolf, C.H., and Robinson, T.E. (1981). Reticulo-cortical activity and behavior: A critique
858 of the arousal theory and a new synthesis. Behavioral and Brain Sciences *4*, 459-476.

859 Vyazovskiy, V.V., Olcese, U., Lazimy, Y.M., Faraguna, U., Esser, S.K., Williams, J.C., Cirelli, C.,
860 and Tononi, G. (2009). Cortical firing and sleep homeostasis. Neuron *63*, 865-878.

861 Vyazovskiy, V.V., and Tobler, I. (2012). The temporal structure of behaviour and sleep
862 homeostasis. PLoS One *7*, e50677.

863 Vyazovskiy, V.V., Tobler, I., and Winsky-Sommerer, R. (2007). Alteration of behavior in mice
864 by muscimol is associated with regional electroencephalogram synchronization.
865 Neuroscience *147*, 833-841.

866 Wimmer, R.D., Astori, S., Bond, C.T., Rovo, Z., Chatton, J.Y., Adelman, J.P., Franken, P., and
867 Luthi, A. (2012). Sustaining sleep spindles through enhanced SK2-channel activity
868 consolidates sleep and elevates arousal threshold. J Neurosci *32*, 13917-13928.

869 Xie, Z., McMillan, K., Pike, C.M., Cahill, A.L., Herring, B.E., Wang, Q., and Fox, A.P. (2013).
870 Interaction of anesthetics with neurotransmitter release machinery proteins. Journal of
871 Neurophysiology *109*, 758-767.

872